J Mater Sci (2011) 46:3766–3776
DOI 10.1007/s10853-011-5290-5

Temperature and surface potential correlations with serrated flow of low carbon steel

A. Yilmaz

Received: 13 July 2010 / Accepted: 14 January 2011 / Published online: 25 January 2011
© Springer Science+Business Media, LLC 2011

Abstract The Portevin–Le–Chatelier (PLC) effect manifests itself as serrated plastic flow in strain controlled tensile tests of dilute alloys. The effect causes most of the material qualities to suffer, including the ductility. Monitoring the effect is important since the induced loss of ductility can cause premature failures on structural materials under load. Surface potential fluctuations of AISI 1020 low carbon steel during its serrated flow was investigated by a combined set-up of an electrochemical cell and a slow strain tensile test. The steel was exposed to an aqueous electrolyte under a strain rate of 1.6 x 10^{-6}/s, and the surface potential was monitored in situ during the creation, magnification, and annihilation phases of the serrated flow achieved by changing test temperatures stepwise between 50 and 85 °C. The serration amplitude showed strong correlations both with test temperatures and the surface potential. A rather large potential shift around 110 mV through active direction during the burst of serrations hinted that the slip bands, in addition to temperature and strain, could also be responsible for the charge release due to the dislocation domains carried in them. The study verifies a potential use of the set-up for monitoring the PLC events in aqueous environments where load cells, extensometers etc. are not utilizable.

Introduction

Plastic flow in metals is explained as nucleation and motion of dislocations [1, 2]. When the dislocation motion is unstable, the flow comes out in strain bursts and arrests on a stress-controlled tensile test curve. Under strains of constant rates and isothermal conditions, the deformation usually appears in serrations of a certain range of frequency and amplitude, which is called the Portevin–Le–Chatelier (PLC) effect. The dependency of the effect on temperature and strain rate has been studied extensively, and observations have shown that the serrated flow occurs when particular strain rates couple with suitable temperatures [2, 3].

In general, the PLC effect induces increase in flow stress, ultimate tensile strength (UTS), and work hardening rate, and decreases the ductility of metals that corresponds to reduction in elongation, effective gauge cross-section area, strain rate sensitivity coefficient, and fracture toughness. The embrittlement induced by The PLC effect is crucial since it leads to unprecedented failures of structural materials [4].

The serrated plastic flow of the PLC effect results in various shapes such as types A, B, and C, depending on where the actual dislocation activities take place in the effective gauge of the specimen. The analysis of serration shapes carried out by Ziegenbain et al. [5] suggested that the serrations observed in carbon steels were dominantly of the type C, in which the effect takes place at random locations of the specimen gauge by activation of fully aged dislocations through local stresses. Recently, several studies have shown transitions among the serration types in some aluminum alloys and carbon steels, which are determined by pyrometric and interferometric techniques on flat specimen surfaces during strain controlled tensile tests [6–8].

Along with the typical dislocation mechanism [1, 9], which is explained as the activation of generated and fully aged dislocations by local stresses, there are other mechanisms proposed via experimental and theoretical

A. Yilmaz (✉)
Department of Chemical and Process Engineering,
University of Yalova, Yalova, Turkey
e-mail: yilmaz5@hotmail.com

approaches for interpretation of the PLC effect [10–14]. Among them, dislocation unpinning from solute atmospheres, dislocation pile ups at grain boundaries, rapid increase of dislocation density and its mobilization at yield, and collective behavior of dislocations are the ones commonly discussed in the literature.

Carbon steels are well known to be sensitive to the PLC effect. It has long been proposed that this sensitivity may come from the high carbon content of the steel. Carbon steels also allow easy permeation of hydrogen which may also interact with the existing solutes such as carbon and nitrogen, and permit all solute atoms to interact with dislocations. In general, the PLC effect is observed in a temperature range where the mobility of carbon atoms is relatively close to the dislocation velocity imposed by strain rate, which supports an interpretation known as solute and dislocation pile-up model [13–16]. According to the model, mobility of solutes such as carbon, hydrogen, and nitrogen becomes comparable to mobility of dislocations under particular strain rates and temperatures. The solutes then may pile up around dislocations and obstruct the smooth transitions between the saturated and enriched local strains in the alloy causing slow and rapid deformation regimes alternately.

There are an ample number of studies aimed at the observation of relationship between serrated flow and a discrete physical event in metal specimens during the PLC effect. Most of the studies have been devoted to techniques such as acoustic emission, thermography, laser speckle pattern interferometry, magnetic flux leakage (MFL) measurements, and digital image correlation (DIC). Each of these techniques has provided important details about mechanisms of this phenomenon.

An analysis of acoustic emission monitoring carried out by Chmelik et al. [9] has shown that each stress drop during a serrated flow corresponds to a movement of at least 10^4 dislocations in any alloy. The speckle pattern interferometry conducted by Zhenyu et al. [7] has revealed dissimilarities in patterns of the PLC band types, and showed transitions among the band types in various alloys. Ranc and Wagner [6] has detected the duration of band formation and the time between consecutive band nucleations precisely using infrared thermography. Using MFL measurements, Dhar et al. [17] have shown differences between Luders band and the PLC bands. According to the study, the flux leakage observed in both bands is due to a decreased magnetic permeability caused by localized plastic deformation. Most lately, an optical technique called DIC has become a common tool for studying band deformation events enabling detection of distinct features of the strain localization of the PLC effect. It provides quantitative data for change of strain fields even within the deformation bands [18, 19].

An electrical field sensor, in other words an antenna, has been used to monitor the serrated plastic flow of aluminum and steel specimens in a fairly recent experimental work of Schmitter [20]. The work confirms the conclusions drawn out of the present work, providing insights about sources of the metal surface (or air–metal interface) charges and charge density fluctuations.

Slow strain rate tensile tests (SSRTs) have been used to make assessments on degradation of metals using dilute aqueous electrolytes at various testing conditions, with or without impressed potentials on tensile specimen surfaces [21–24]. Despite the tests are ample, there are no more than a few reports on fluctuations of electrochemical parameters of alloys during the PLC effect. A fairly recent work, carried out by Darowicki and Orlikowski [24], showed the effect of impressed potentials on electrical impedance behavior of an aluminum tensile specimen during the PLC effect. The work concluded that the change on the impedance during the PLC effect was more significant when a lesser passivity of the alloy was achieved, i.e., when the surface oxide films were thinner.

There has been no report on direct monitoring of surface potential of a metal together with magnitudes of its serrated flow. The method presented is useful as a potential tool for monitoring the PLC effect, and checking deformation and damage progress in laboratory settings for metals susceptible to the PLC effect. The experimental set-up and measurements are relatively simple and applicable to investigate other metals and alloys intended for use in aqueous environments. The work presents an electrochemical signature recorded during the PLC effect of carbon steel and discusses about possible sources of this charge release, with no aim for interpretation of the effect, or supporting of any of those models that exist in the literature.

Experimental

Test equipment

The test cell schematic shown in Fig. 1 was glass blown in 1-L capacity. It consisted of seven joints at the top, and one joint at the bottom. The joints located centrally and axially received cylindrical LCS tensile specimen via Teflon o-rings and Nylon threaded fittings as sealed. Only the upper root of the specimen had moved with a minimal friction, which did not affect the stability on the load measurements. The cell safely contained the ground water test electrolyte and the cell elements during the SSRT tests. The joints around the central top neck were designed such that the cell elements could be easily inserted and held in the electrolyte. A water-cooled reflux condenser fitted into

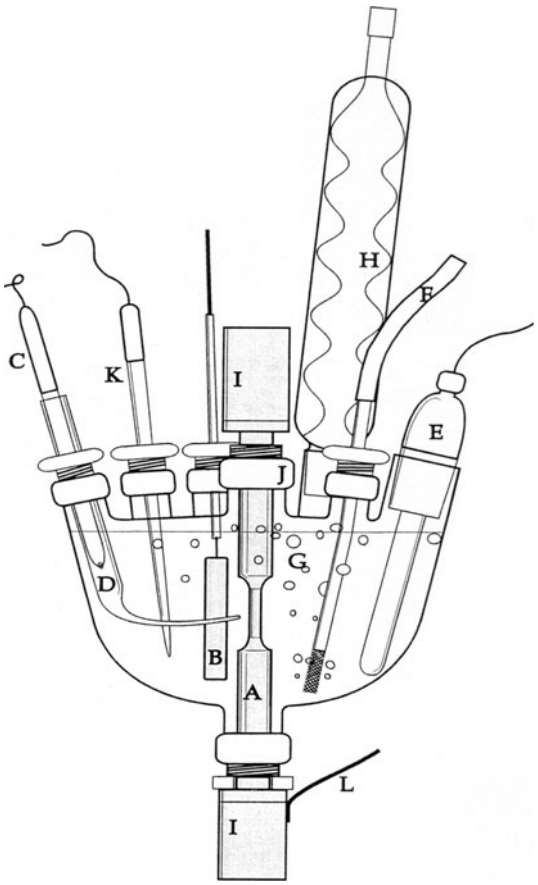

Fig. 1 Schematic of the test cell with installed specimen and the rest of the cell elements: *A* specimen-working electrode (WE), *B* platinum counter electrode, *C* saturated Ag/AgCl reference electrode, *D* Luggin probe, *E* quartz immersion heater, *F* fritted-end purging capillary, *G* electrolyte, *H* water-cooled condenser, *I* universal joints, *J* threaded joints with o-ring seal, *K* thermo-well, *L* electrical connector to WE

one of the large stop joints minimized possible solution loss due to evaporation at high temperatures. Heating of electrolytes were done by a quartz electric immersion heater (LHP 100, Glo-Quartz Elect. Co), specifically designed for environmental experiments. A fritted glass end capillary was used for purging gas into the test solution. De-aeration of the test solution was maintained by continuously purged nitrogen gas at a rate of 150 mL/min. A glass blown Luggin probe made out of a Pasteur pipette was inserted into the cell via an o-ring fitting, in which the reference electrode (saturated Ag/AgCl) was held in a fixed position. The tip of the Luggin probe was maintained at a fixed distance from the specimen surface (2 mm). A sealed-end Pasteur pipette thermo-well enclosed the thermocouple, which was also held near to the test specimen. A large (10 cm^2) platinum sheet sealed onto a glass capillary was used as a counter (auxiliary) electrode to supply good current distribution in the cell. A PID temperature controller with the immersion heater maintained desired test temperatures within an accuracy of $\pm$ 0.1 °C. A screw-drive-mechanism universal testing machine (United Calibration Corp, Model STM-10E-S) was used for the entire electro-mechanical tests that were exclusively designed for slow strain rate testing (SSRT) with 2 kN load cell mounted under the moving cross head, over the test cell. A Pentium based custom made computer (Southern California Computers, Model PAC-1200/PCI-10S) with data processing software and hardware (United Calibration Corp., Datum for Windows, Version III) were used for stress–strain curve scanning. The universal machine enabled any desired strain rate between 10^{-8}/s and 10^{-2}/s. A Gamry model potentiostat (Gamry Instruments, PC4 (750)/DC105 II) was used for monitoring potential over tensile test specimens in the test cell.

Microstructure

Metallographic analysis on the low carbon steel specimens of 0.08 weight % carbon content revealed a microstructure which comprised approximately 85% ferritic and 15% pearlitic grains. Pearlite grains formed out of typical lamellar structure showed a slight alignment in the axial direction (pulling direction) of the finished test specimens, which manifested cold or hot rolling process done on the steel. The average grain size was measured to be 21 microns, and its distribution throughout the specimen was fairly even. Micro-hardness tests conducted with a Shimadzu model optical micro-hardness tester revealed significant differences in hardness of pearlite and ferrite structures as expected. Vickers hardness numbers were calculated as 374 and 270 for pearlite and ferrite grains, respectively, out of diagonal measurements of diamond indentations. Several micro-hardness tests were carried out over individual pearlitic grains at different regions of the specimen, to detect involvement of any bainite in the pearlite structures. However, all tests conducted over different domains of individual grains revealed the same Vickers number given above, showing no other harder or softer substructure involvement in those pearlite grains. Specimens polished with final 0.05 micron diameter alumina powder revealed spherical type inclusions of $\sim$1 micron diameter. Electron dispersive X-ray analysis of the inclusions by a cold field emission scanning electron microscope (Hitachi, S-4700) revealed high peaks of manganese and sulfur, which was verification of MnS non metallic inclusions commonly found in variety of low carbon steels.

Specimen and electrolyte preparation

Cylindrical specimens of the chemical composition given in Table 1 were machined out of a low carbon steel slab within a tolerance of 5/1000 inches in diameter and length

Table 1 Weight % chemical composition of low carbon steel

Element	C	Mn	P	S	Si	Cr	Ni	Cu	Mo	Fe
LCS	0.08	0.84	0.02	0.05	0.12	0.08	0.09	0.34	0.03	Bal

of the effective gauge. The length of the specimen (~6 inches) was designed to fit in the environmental cell as the threaded ends were exposed out of the test cell, and can be connected to the universal joints, as shown in Fig. 1. The effective gauge length was machined to 0.640 inches with a corresponding gauge diameter of 0.160 inches. Teflon (PTFE, polytetrafluorethylene) tape wrapped around the specimen exposed only the effective gauge surface area for potential scanning in the test solution. The gauge was manually ground with successive finer SiC emery papers until the 600 grit finish. The specimen surface was degreased with acetone, and washed with water, and rinsed with alcohol and distilled de-ionized water (DDW). Then, it was rapidly installed into the test cell and exposed to the test solution conditioned by nitrogen gas for 2 h.

The test solution (ground water) of the chemical composition given in Table 2 was prepared by mixing the appropriate formulated chemicals with DDW initially kept at 35 °C. First, the chlorides and sulfates were mixed with DDW, and then the bicarbonates and silicates were added in appropriate amounts. The solution was taken out by siphoning over the insoluble precipitates accumulated in the bottom of the flask, and filtered by No. 52 (Whatman Qualitative) paper to reach a clear and colorless electrolyte. The pH of the ground water test electrolyte was measured to be 8.0, as slightly alkaline. Then, the solutions were conditioned (de-aerated) by purging nitrogen gas for at least 2 h before specimen immersion.

Test procedures

Slow strain rate tests of LCS for investigating the PLC effect was carried out at a strain rate of 1.6×10^{-6}/s at various temperatures between 50 and 85 °C. The strain rate was determined by several initial tests, by iterations of various rates from 1×10^{-7}/s to 1×10^{-5}/s at 85 °C, to achieve maximized serration amplitudes. Freshly prepared wet-ground specimens with a final 600-grit emery paper were installed into the cell through the central necks using o-ring compression fittings. Then the conditioned de-aerated water was transferred to the test cell within 10 to 15 s without excessive exposure to the air, and the cell joints were closed rapidly by inserting the entire elements of the cell as sealed. The installation of the cell on to the universal joints did not exceed a total of 4–5 min after the specimen installation. After that, de-aeration by purging nitrogen gas at a constant flow rate of 150 ml/min was started, which was continued till the failure of the specimen. After setting the temperature controller and heating unit, open circuit potential monitoring of LCS was started. The open circuit potential (E_{corr}) was stabilized around -600 $mV_{Ag/AgCl}$ in ~1.5 h as the temperature reached to the desired value of 85 °C to an accuracy of ± 0.1 °C. The specimen was strained until roughly a mid-point of YP and UTS in the plastic region. Then, the SSRT was started with prearranged strain rate of 1.6×10^{-6}/s for maximized serration amplitudes. The interface potential was scanned as test temperature was changed in steps of 5 °C, approximately in a period of every 2 h, until the failure of the specimen. It took only 2–3 min for a test temperature to shift to a new stabilized value after each switching. After the failure, specimens were uninstalled and examined under a stereo microscope for any corrosion attack, and pH change of the test solution was recorded.

Table 2 Chemical composition of the test solution; pH: 8.0

Ions	Na^+	SiO_2	Ca^{2+}	K^+	Mg^{2+}	$HCO3^-$	Cl^-	$SO4^{2-}$	F^-
mg/L	61.3	70.5	101	8.0	17.0	200	117	116	0.86

The present SSRT-electrochemical tests have been repeated several times. All of them showed a similar trend in the style of correlations among temperature, serration amplitude, and surface potential. Since parameters such as the specimen heat, solution concentration, passive film formation, and the initial electrochemical conditioning etc. would slightly be different for each test batch, the potential values and other data would come out in slight differences. Thus, comparison of those separately carried out tests has been avoided. Instead, one representative experiment of a single specimen has been presented, where the oneness of electrochemical, mechanical, and inherent parameters of the test specimen is not questionable.

Results and discussions

Differences in mechanical behavior at 25 and 85 °C

The stress–strain curves obtained by the SSRT at 25 and 85 °C under a strain rate of 1.6×10^{-6}/s showed dissimilar features in flow types and tensile test parameters. The curve of 25 °C given in Fig. 2 revealed a regular plastic flow with a sharp yield point. On the contrary, the entire plastic region of LCS became a serrated flow of type C at 85 °C, in which the localized deformation bands hop arbitrarily in the specimen gauge [5]. The UTS at 85 °C was approximately 100 MPa higher than that at 25 °C, as shown in Fig. 2. The engineering failure stress point at 85 °C was also higher, approximately in the amount of

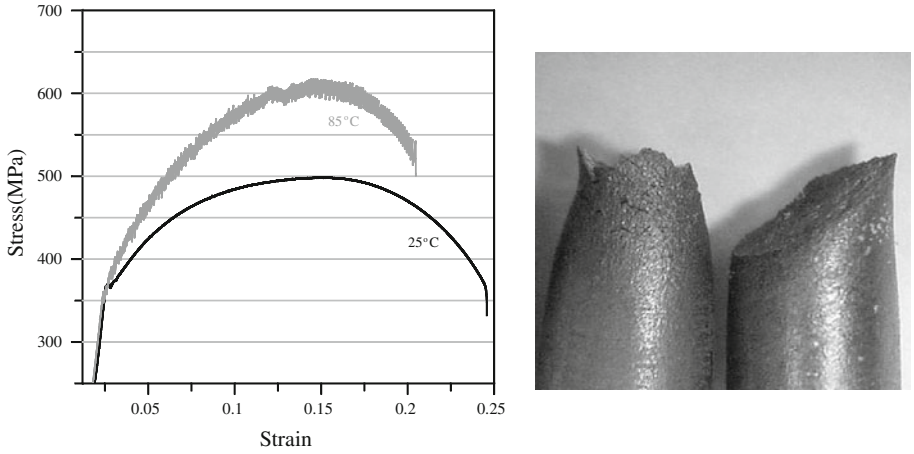

Fig. 2 *Left* Stress–strain profiles of LCS by SSRT conducted at a rate of 1.6×10^{-6}/s at two different temperatures. *Right* Corresponding ductile and brittle failure features of LCS, respectively at 25 and 85 °C

200 MPa. The differences may become much lower when nominal strains are considered, by including the gauge sections of the failed specimens. The yield point of LCS did not show any significant change with temperature increase from 25 to 85 °C. At 25°C, the specimens showed ductile behavior with approximately 25% elongation revealing a typical necking of the specimens shown in Fig. 2. The specimens at 85 °C did not show any significant necking. They experienced rather brittle failures with planar crack surfaces of an oblique angle approximately 45° to the load direction. Specimens showed no visible corrosion attack under their protective passive films at either of the test temperatures.

The examined range of the load-elongation curve of LCS under temperatures from 50 to 85 °C at a strain rate of 1.6×10^{-6}/s is given in Fig. 3. This range, extending from the YP–UTS midpoint to the failure point, allowed various temperatures to be applied and tested in steps of 5 °C within reasonable time intervals. When temperature was dropped abruptly from 85 to 50 °C, as shown in Fig. 3, the serrated region became a smooth line of a typical regular plastic flow. No further change in the flow character was recorded as the temperature was kept constant at 50 °C. With a temperature rise of 5 °C, the curve started to show serrations of detectable minimum amplitude. The average amplitude of the serrations, again, stayed unchanged as the temperature was constant at 55 °C. At each temperature increment of 5 °C, the average amplitude of the serrations was increased to a new level, and reached back to the initially recorded highest amplitude at 85 °C.

The load drop during the change from 85 to 50 °C shown in Fig. 4 is a natural response to the non-serrated (regular) plastic flow that has just been reached. Since the UTS point with the PLC effect was approximately 100 MPa higher, as seen in Fig. 2, it just had to drop back to those values that belong to the non-serrated curves where the PLC effect is absent. Accordingly, the stepwise increase in temperature recreated more PLC events that

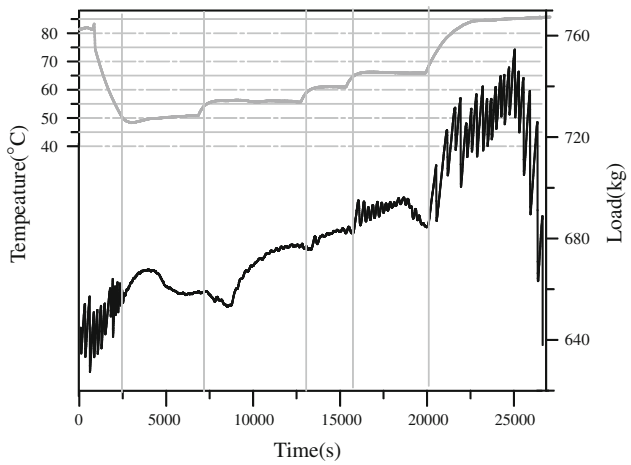

Fig. 3 Transitions of serration amplitude with changing test temperatures during SSRT of LCS at a strain rate of 1.6×10^{-6}/s

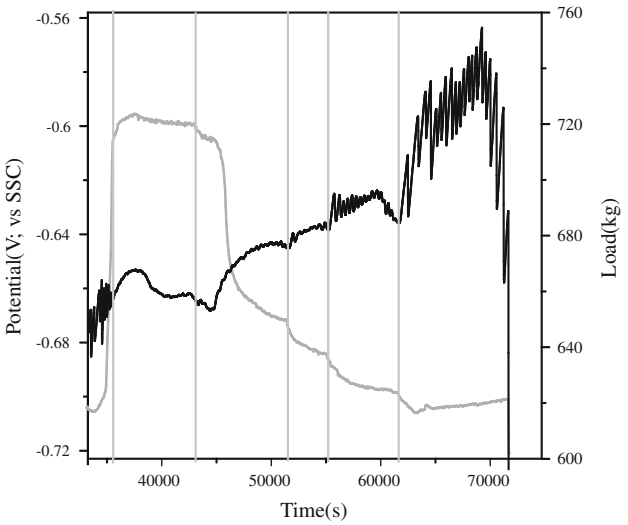

Fig. 4 Correlations of surface potential (metal–electrolyte interface potential) with the serration amplitudes of the PLC effect in LCS at a strain rate of 1.6×10^{-6}/s

accompanied with more load increase toward the original UTS point of the serrated curve observed at 85 °C. There seem to be a more fluctuation in the serration behavior at 65 °C. However, this is expected since the temperature fluctuations in the specimen might not have been controlled precisely, which sometimes reach to a couple of degrees, as can be deduced by examining the entire region tested. Otherwise, the tests display a fair relationship between the average serration amplitude and the deformation stress.

The interface potential was scanned to determine its transients during the stepwise increase of temperatures from 50 and 85 °C in steps of 5 °C by which more amplified serrations were set in. The tests showed strong correlations among all of the three parameters; test temperature, serration amplitude, and the potential transients, as shown in Fig. 4. By a temperature drop from 85 to 50 °C, by which the serrations were annihilated, i.e., the deformation became a regular plastic flow, a sharp increase in the potential toward the noble direction was observed. This potential shift of ~110 mV occurred when switching from the serrated flow of the largest amplitude at 85 °C to non-serrated plastic flow at 50 °C, within a temperature change of 35 °C. The observed potential shift is rather large when compared with previously reported surface potential fluctuations of non-strained steel as a consequence of temperature variations [21].

The potential shift was the highest during the creation of serrations, as seen in Fig. 4, between the non-serrated flow and weakly serrated flows. While serrations started at 55 °C with the least repetitive fluctuations in load, approximately an increase of 70 mV in interface potential was registered. This particular segment attracts attention since it is the largest portion of the entire shift of ~110 mV, which occurs between non-serrated and a weakly serrated flows. After the onset of serrations, more temperature increase brought about more amplified serrations with accompanying higher interface potentials. This continued until reaching the original amplitude of serrations, and initially observed highest surface potential. Both the achieved highest serration amplitude and the interface potential stayed nearly unchanged until the failure. Another noticeable point, as seen in Fig. 4, is the saturation of the segmental potentials to a stable value within ~1.0 h, at any of the test temperatures applied.

Consequently, switching from the regular flow to the serrated flow achieved by changing test temperatures revealed a large (110 mV) shift in the interface potential of the LCS. The shift was toward the active direction, which was about population of extra electrons at the metal–solution interface. The correlations observed among serration amplitude, test temperature, and measured interface potential can be consequence of various sources. Intrinsic qualities of a specimen such as shape, size, surface roughness, microstructure, etc. are basic influential factors on the serrated flow, and they are expected to alter the surface potential as well. Temperature is another effective parameter on the surface potential due to its drive on the activation energy change of reactions at a passive layer–solution interface. On the other hand, factors such as strain, slip plane exposure to the electrolyte due to the serrated flow of the PLC effect, and the charge separation events of the passive oxide layer at the interface can contribute to the observed potential shift in a large extent.

Effect of specimen qualities and microstructure

Effect of specimen thickness on serrated flow of the PLC effect in aluminum alloys has been investigated by Ziegenbein et al. [25], a prominent group in the study field. The study showed that the average localized band strain was independent of the specimen thickness, while there were some associations between a particular PLC band type and its average strain. The PLC band widths in the study have been found to be increasing proportionally with the specimen thickness. Similarly, the experiments conducted by Zhang et al. [26] using cylindrical specimens of different diameters under various imposed strain rates have shown an increase in band width in proportion to the specimen diameter, where the proportionality constant for diameter to band width ranges from 1.5 to 2.0. The results of those studies would imply that nucleation, development, and propagation rate of the PLC bands are independent of the specimen size. Therefore, the PLC banding events or the corresponding serrations are controlled by some inherent mechanisms such as dislocation correlations, rather than by a mechanism like necking limitation associated with specimen size.

Plastic flow instability of Al tensile test specimens is increased when the ratio of specimen perimeter to its cross sectional area gets larger, in an experimental work of Zdunek et al. [27]. The work has revealed that The PLC effect was pronounced more with T-shaped, rectangular, and square specimens than with round ones. This may be in connection with the effects of edge and corners, on which a PLC band nucleation by some mechanism can take place relatively easily. Thus far, there has been no report on correlation of band types either with specimen shape and thickness, or with band width.

In fact, specimen size on the measured surface potential is expected to have no influence, both for a stationary specimen and a one under tension. Any specimen, small or large, has an interface with test electrolyte as large as its own surface area. For any specimen size, interface potential due to electrochemical interactions of a particular alloy–electrolyte system will be the same then, due to the unchanging ratio of the interacting surfaces of metal and

electrolyte. However, the surface potential measurements in an electrochemical cell, that has to be carried out by a Luggin probe, require a certain attention on the specimen size, especially in a case where an extra potential coming out of a non-electrochemical interactions to be measured, like in the present work. For small specimens, Luggin probe tip can be kept in a close proximity with entire surface of the specimen gauge, So that a charge release at any point away from the tip can be detected decently. This is not quite valid for large specimens, as the potential reading becomes smaller than the amount of a charge release at a far point from the tip. Therefore, small specimens (small surface area exposure to the electrolyte) and close probing of the surface bring out a measurement sensitivity on the surface potential changes which help correlate the PLC events accurately.

In general, smaller grain sizes have been found to promote larger PLC serration amplitudes. For instance, according to a series of tests conducted with some Al–Mg alloys the effect of grain size becomes greatest toward the ultrafine nanocrystalline sizes [28]. Other experiments carried out with a number of variously treated alloys revealed severe serrations for the solution-treated ones [29], where some of the peak aged alloys showed no serrations. For reversion-treated specimens, the serrations were continuous throughout the plastic range. The results of the same study showed that the plastic flow of the studied Al–Li alloy was dependent of not only its microstructure, but also its texture. Besides, grain size distribution was also found to be an influential factor on the plastic flow by Hahner [30]. The results of his study imply that evenly distributed grains promote more serrated flow. According to the study, there would be more stress incompatibilities between neighboring grains of an uneven grain distribution, which do not make a relevant propagation mechanism available for the localized bands.

In general, surface potential difference is attributed to differences on geometrical surface areas in contact with electrolytes, as long as the electrolyte concentration, chemical composition of tested alloy, and test temperature stay constant. Therefore, a change in grain size may not have a significant effect on surface potential of alloys, unless it results with notable change in alloy composition to alter the interactions at alloy–electrolyte interface. No detailed work has been reported so far on the topic.

Influence of crystal orientation has already been investigated using micro-indentation of individual grains [31]. The studies have shown that the unstable flow is pronounced more when the direction of indentation is close to the crystallographic orientation <100>; in other words, when the diagonal of the indenter of Vickers test coincided with the <110> direction. Solution-treated and peak aged 2090 Al–Li alloys have also revealed interesting results regarding the crystal orientation effect [29]. While no serrations were observed in the central section of the studied specimen, the surface layer which was oriented differently relative to the center showed serrations. However, these results were not strongly affirmed by others [32] since specimen orientation was not found to influence the magnitude of the serrations in solution-treated aluminum alloy specimens.

The PLC effect susceptibility of alloys depends on the surface finish too. For instance, unpolished aluminum alloy specimens in a tensile test serrated fairly, while the specimens polished to 3000 grit or more had perfectly smooth tensile curves at a particular strain rate and temperature [33]. The study emphasized that the rolling of metal sheets increases their surface roughness and that these defects on the specimen surface constitute stress raisers on which the nucleation of PLC bands may be induced. The authors also found out that the bands of the polished specimens propagated about twice as fast compared with those of the unpolished ones in stress-controlled tensile tests. Thus, the band propagation velocity, among the other parameters, strictly depends on the surface quality of the specimens. When surface quality was inferior, the range of temperatures and strain rates over which the PLC effect occurs became greater, as reported by the same work. This is consistent with implications of other studies [34], where a strong correlation between the localized strain of the PLC bands and specimen surface roughness has been verified via con-focal microscopy.

Surface finish greatly controls the specimen surface area in contact with electrolytes. This area can easily be increased by several times, roughening the surface with coarse emery papers for instance. Indeed, the electrochemical test specifications established for surface finishing serve for this important reason. A large surface area of coarse finish would reveal a much higher interface potential than a smooth fine finish. Thus, a small potential addition to the higher interface potential of the rough surface is detected with less accuracy, due to the larger difference in between the background potential and the newly emerging one at the interface. While increased roughness negatively affects measurement ability of Luggin probe, specimens with rough surfaces promote more serrations to the contrary, as discussed earlier. Therefore, a moderate polish (around 600 grit with silicon carbide emery papers) would suffice for detection of serration–surface potential correlations, as done with the present work.

Strain effect

When an alloy is strained within the elastic range, the strain energy added into it persists as long as the stress is applied. This process is mechanically reversible; the energy will be

restored when the stress is removed. However, if the strain exceeds the elastic limit, the process becomes mechanically irreversible and the residual strain energy remains in the specimen during and after the applied stress. When such an alloy during its regular plastic flow is immersed in an electrolyte, it takes up a "mixed potential", and corrosion proceeds by a changed new corrosion potential [35]. On the other hand, when the alloy is protected by an intact passive film during a straining under slow rates, the potential change is expected to be similar to that of a non-strained specimen. The slow strain rates allow time for the film healing processes which do not let the residual strains of the metal surface be exposed to the electrolyte.

An early experiment has proven that the straining of a specimen in the plastic range of regular flow does not change the surface potential significantly unless the passive film is ruptured [36]. In the work, different shapes of wires strained at medium rates produced potential time curves of four different forms. However, all wires gave the same strain–time curves when tested with high speed photography. The strain–time curves were related to the overall strain of the specimen, whereas the potential resulted from the strain on the passive film and its consequent ruptures. Besides, a work [37] compared the potential of carbon steel cleaned by blasting with that of un-deformed steel. The difference in potential is found to be about 50–70 mV at a direct current of 10 mA/cm^2, as mostly attributed to the difference on the geometrical surface areas in between. The potential on the un-deformed steel was measured to be more noble in that study.

Temperature effect

Temperature is a well-known parameter chiefly influential on the chemical reactions. In our work too, the effect of temperature change on the potential shift is plausible. In general, the activation energy of a chemical reaction is directly related to the temperature. Thus, temperature in corrosion reactions tends to increase the critical anodic current density. This general attitude of temperature can explain the present observations on the potential shift, which is conveniently toward the active direction. However, it looks difficult to make sure by any procedural means whether all 110 mV shift would result from the temperature. It becomes even more difficult when the segmental change of $\sim$70 mV for only 5 °C change in temperature is considered, as seen in Fig. 4, which suggests a possible involvement of some factors other than, or in addition to the temperature. Some reports of prominent authors in corrosion field such as Fontana and Greene and Jones [38, 39] state that temperature has usually a little affect on passive metallic dissolution rate and the primary passive potential, as may hint on some other sources for the detected rather large surface potential of our case.

The temperature effect on the non-strained carbon steel specimens has already been investigated in a preliminary study carried out under the same environmental conditions [21]. The study showed that the anodic dissolution of the steel was hindered more in colder (25 °C) ground water electrolytes giving rise to cathodic reaction rates, which in turn raised the corrosion potential (interface potential). In other words, at the hot (85 °C) ground waters the interface potential was shifted toward the active direction suggesting a dissolution process of the steel, according to the "mixed potential" theory. The difference in the interface potential of the steel for a temperature change from 25 to 85 °C in that work was found to be 30–35 mV.

Another means to predict the effect of temperature can be the analysis of the Tafel equation, a half portion of the Nernst equation, for a particular reaction type such as anodic or cathodic. The relationship between reaction rate and interface potential for activation polarization is given with the Tafel equation as in the following:

$$E = 2.3RT/anF \log I/I_0 \quad (1)$$

where E is over-potential, R is the universal gas constant, T is absolute temperature, n is the number of electrons transferred, F is the Faraday constant, I is the rate of oxidation or reduction in terms of current density, and a is the symmetry coefficient which describes the shape of the rate-controlling energy barrier.

One can estimate the changes in the polarization with reaction rate when a plot of over-potential against current density of Tafel equation shown above by attributing a most common value of 0.1 V for the term $\{2.3\ RT/anF\}$ for simplicity. This value, which is the slope of the linear Tafel equation, is about 0.12 V for the carbon steel-ground water system in the present study. According to the equation, the reaction rate then changes *by one order of magnitude for each 100 mV or 0.1 V shift in the over-potential*. This shows that the rate of an electrochemical reaction is very sensitive to small changes in the interface potential. However, the opposite is not valid; a great change in the reaction rate affects the interface potential to only a small degree.

The reaction rates of the non-strained specimens in the previous report [21] are 45 and 150 μpy, respectively, for 25 and 85 °C, for a potential shift of 35 mV. These figures are matching fairly in the expected surface potential values and reaction rates when the Tafel equation is considered. However, it is difficult be convinced whether a potential shift especially of $\sim$70 mV can result with seven times as much corrosion rate, can result from only a change of 5 °C at the segment between 50 and 55 °C in the present study.

Therefore, the results are suggestive to look for other effective sources on the observed interface potential shift.

The slip plane events

Regular flow

In a test exhibiting a regular non-serrated flow, the plastic deformation is distributed evenly in the entire effective gauge of the specimen. This homogeneous flow resumes until necking of the specimen at the point of the UTS, where a localized deformation starts to takes place. A local deformation in any particular section of the specimen until necking is only a very small fraction of the deformation at the whole gauge. A passive film on such a material showing regular flow may be affected in various manners depending on the strain rate, film brittleness, electrolyte ionic concentration, corrosion potential, etc.

The competitiveness between the rates of regular plastic deformation and passive film healing (re-filming) determines the film rupture events. When the deformation rate is dominant, the films may be ruptured in some arbitrary time intervals until they cannot withstand with the exerted tensile force on them during the testing. After a rupture, the film may try to heal itself as the plastic deformation of the alloy continues, and may become intact again in the favorable strain rate and electrochemical conditions. When a specimen is pulled with a high strain rate, the film healing may become relatively slow that it can experience another rupture before a complete healing. This may also follow consecutive ruptures at various points of the gauge when the rate is high. However, it is quite possible for a passive film not to be ruptured when the plastic deformation rate is slow enough. There, the relative high healing rate of the film is capable of fixing the damaged areas before a full rupture occurs. Thus, a passive surface film of a regularly deforming alloy under very slow strain rates has a good chance to stay intact for a reasonable time period.

Serrated flow

The serrated plastic flow comes out of the localized plastic deformation of the PLC effect. In this particular flow, the local deformation region on a specimen appears in a band shape of an oblique angle to the load direction, and it moves along the gauge. Each nucleation, formation, and motion of these bands corresponds to a load drop in a strain-controlled tensile test curve. Then, the stress strain curve becomes serrated when the banding events are repeated under the same testing conditions.

A passive film of an alloy experiencing a serrated flow is affected differently. The plastic deformation through those localized bands has much larger local magnitude compared to that of the regular flow. Each time, when a band event ends up with the slip action along the slip line, the emerging out slip step can easily rupture the passive film on the specimen. This can be pronounced much more when especially the film is brittle and thin. Then, the fresh (non-filmed) specimen surface exposed to the electrolyte can have an influence on metal–electrolyte interface potential. After such slip-induced rupture, the film may start to heal by some rate depending on the electrochemical parameters of the metal–electrolyte system. However, another rupture may occur elsewhere on the gauge with a newer slip step event. Thus, there is a continuous presence of some fresh metal surface area exposure to the electrolyte as long as the test parameters remain the same. Otherwise, altered parameters will affect the re-filming rate and the slip step events, causing change in the exposed metal surface area to the solution.

It is known early that the formation of dislocations by cold work or strain aging increases electrical resistance in metals [40]. An edge dislocation, for instance, contains extra planes of ions above and below the slip plain, which are the bound states where the conduction electrons are trapped [41, 42]. During a serrated plastic flow or the PLC effect, the emerging slip steps expose the dislocation core domains at the metal–electrolyte interface, as the oxide layer is ruptured. Hence, the stress field around dislocation cores cause change in electron density, which then becomes detectable as a change in the interface potential (metal surface potential).

The findings over the slip step events have been confirmed by a study conducted by Schmitter [20], by means of an antenna surrounding a steel tensile test specimen in air. The work showed detectable electric field fluctuations on the specimen surface, which was due to a change in the surface charge density during the PLC effect. Another work conducted by Darowicki and Orlikowski [24] reports impedance changes of an aluminum specimen surface film tested under imposed potentials during serrated flows. The work shows that lower passivation rates allow observe the phenomenon better, which supports the findings of this work; as thinner films are easily ruptured by the emerging slip steps into the electrolyte to raise the potential that comes from the dislocation cores.

Consequently, a fair amount of contribution to the observed potential shift may come from the slip step events of the PLC effect. An increase in test temperature increases the serration amplitude by activating more serrated flow, as the PLC effect is solely temperature dependant at the constant strain rates. Then, the resultant local deformation bands can emerge into the electrolyte rupturing the passive film. Then, the resultant localized bands emerge into the electrolyte rupturing the passive film. Each increase in

temperature increases the number of ruptures, creating a larger fresh surface area with more trapped electrons at those bound states in the slip planes, which can be detected as an extra potential reading at the metal–solution interface via a Luggin probe, like in the present set-up.

Passive oxide layer charge separation

The oxide layer charge separation during the film rupture, in addition to straining, temperature, and dislocation charge densities on the exposed metal surface, can be a contributing factor too for the observed potential shift [43]. The typical potential values resulting from the effect are generally low and may not be comparable with that of the sources given above unless the oxide layers are pounded by energetic photons such as pulsed laser etc. Despite that, emission of photo-stimulated electrons from the oxide layers should not be totally excluded. Because the present experiments are done with no isolation of the test cell against the light of the testing laboratory, and a film rupture is always expected at each slip step emerging of the irregular flow. The contribution ratio between slip step events and the charge separation events may be examined by measuring the total slip step surface area which is expected to be proportional to the detected potential of dislocation cores.

High temperature and strain rate applicability

In general, the serrated flow peak shifts to higher strain rates at higher temperatures. Mobile dislocations stimulated by higher strain rates are faster. Then, a higher temperature is required to increase solute diffusivity to a comparable value of the higher dislocation mobility, for the solute-dislocation interactions to occur. Thus, alloys showing serrated flow at higher temperatures are being subjected to higher strain rates in general. Due to this nature of the PLC effect, it seems the set-up would still be useful to correlate the serrations with the interface potential at temperatures around 300–400 °C, and at corresponding rates around 10^{-3} to 10^{-2}/s. The film at the interface is likely to be the only restriction, as discussed earlier, which should be brittle enough to be failed by slip steps of localized bands, and should have fast healing ability under electrochemical conditions of the tests. When this is on hand, higher oxidation rate at higher temperatures will cause a thicker film formation on alloy surfaces which may not be failed by higher strain rates due to the temperature-induced faster film healing rate. Non-passivating alloys, which tend to corrode more at high temperatures, should not be considered as candidate materials for the tests, while acquisition of a meaningful data on serration–potential relationship depends on the described passive film character. Intended higher test temperatures may need some physical modifications on the set-up; however, higher strain rates may not require any. Lesser oxygen solubility at higher temperatures may avoid the de-aeration done with an oxygen free gas in the present work. Also, the test cell, reference electrode, and Luggin probe may be made out of high temperature resistant materials, such as Teflon and its derivatives.

Conclusions

The present tests carried under a slow strain rate of 1.6×10^{-6}/s showed susceptibility of the LCS to the PLC effect starting at a temperature of $\sim$55 °C. The serration of the PLC effect was amplified by raised test temperature and reached up to a typical C type serration at higher temperatures. The surface potential of the steel during this change showed strong correlations with both the temperature and the serration amplitude. Four parameters such as strain, temperature, slip plane emergence to the electrolyte, and oxide layer charge separation events have been thought to be responsible for the subject potential shift. Among them, the dominant contribution to the shift was attributed to the temperature and slip line events of the serrated flow. It looks possible for the set-up to be used as a new technique for investigation of the PLC effect, if the slip line events contributing to the potential shift become separable from the other effective factors. The set-up can be used as an in situ monitoring device to study the PLC effect in aqueous environments, where load cells or strain gauges are not utilizable. The set-up is appropriate for the high temperature investigations, and may help detect damage progress to avoid unexpected failures of load bearing materials susceptible to the PLC effect.

Acknowledgements I would like to extend my gratitude to Professor Dr. Dhanesh Chandra, at The University of Nevada, Reno in the Department of Metallurgical and Materials Science and Engineering, for all facilities and necessary equipment and devices made available, and for invaluable discussions contributed to the work. I would also like to extend my gratefulness to Dr. Stephan Fuelling, at The University of Nevada, Reno in the Department of Physics, for reading the manuscript.

References

1. Cottrell AH (1953) Dislocations and plastic flow in crystals. Oxford University Press, London
2. Keh AS, Nakada Y, Leslie WC (1968) Dislocation dynamics. McGraw-Hill Press, New York
3. Penning P (1972) Acta Metall 20:1169
4. Wagner D, Moreno JC, Prioul C, Frund JM, Houssin B (2002) J Nucl Mater 300:178
5. Ziegenbain A, Hahner P, Neuhauser H (2001) Mater Sci Eng A 309:336

6. Ranc N, Wagner D (2008) Mater Sci Eng A 474:188
7. Zhenyu J, Qingchuan Z, Huifeng J, Zhongjia C, Xiaoping W (2005) Mater Sci Eng A 403:154
8. Huifeng J, Qingchuan Z, Xuedong C, Zhongjia C, Zhenyu J, Xiaoping W, Jinghong F (2007) Acta Mater 55:2219
9. Chmelik F, Klose FB, Dierke H, Sachl J, Neuhauser H, Lukac P (2007) Mater Sci Eng A 462:53
10. McCormic PG (1988) Acta Metall 36:3061
11. Onodera R, He ZG (2002) J Jpn Inst Met 66:1048
12. Kubin LP, Estrin Y (1991) J Phys III 1:929
13. Fressengeas C, Beaudoin AJ, Lebyodkin M, Kubin LP, Estrin Y (2005) Mater Sci Eng A 400:226
14. Lebyodkin MA, Brechet Y, Estrin Y, Kubin LP (1995) Phys Rev Lett 74:4758
15. Thevenet D, Mliha-Touati M, Zeghloul A (1999) Mater Sci Eng A 266:175
16. Mulford RA, Kocks UF (1979) Acta Metall 27:1125
17. Dhar A, Clapham L, Atherton DL (2002) J Mater Sci 37:2441. doi:10.1023/A:1015419018741
18. Bruck SA, McNeill SR, Sutton MA, Peters WH (1989) Exp Mech 39:261
19. Zavattieri PD, Savic V, Hector LG, Fekete JR, Tong W, Xuan Y (2009) Int J Plast 25:2298
20. Schmitter ED (2007) Phys Lett A 368:320
21. Yilmaz A, Chandra D, Rebak RB (2005) Metall Mater Trans A 36:1097
22. Shaffer TF, Revie RW, Mandal A (1995) Radioact Waste Manag 21:696
23. Szklarska-Smialowska Z, Xia Z, Rebak RB (1994) Corros Sci 50:334
24. Darowicki K, Orlikowski J (2007) Electrochim Acta 52:4043
25. Ziegenbein A, Hahner P, Neuhauser H (2000) Comput Mater Sci 19:28
26. Zhang Q, Jiang Z, Jiang H, Chen Z, Wu X (2005) Int J Plast 21:2150
27. Zdunek J, Spychalski WL, Mizera J, Kurzydlowski KJ (2007) Mater Charact 58:46
28. Wagenhofer M, Erickson-Natishan MA, Armstrong RW, Zerilli FJ (1999) Scr Mater 41:1177
29. Shen YZ, Oh KH, Lee DN (2004) Scr Mater 51:285
30. Hahner P (1993) Mater Sci Eng A 164:23
31. Kovacs ZS, Chinh NQ, Lendvai J (2001) J Mater Res 16:1171
32. Shabadi R, Kumar S, Roven HJ, Dwarakadasa ES (2004) Mater Sci Eng A 382:203
33. Abbadi M, Hahner P, Zeghloul A (2002) Mater Sci Eng A 337:194
34. Kang J, Wilkinson DS, Embury JD, Jain M, Beaudoin AJ (2005) Scr Mater 53:499
35. Clarke M (1970) Corros Sci 10:671
36. Roberts KJ, Shemilt LW (1969) Trans Inst Chem Eng 47:204
37. Lewis D, Northwood DO, Pearce CE (1969) Corros Sci 9:779
38. Fontana MG, Greene ND (1978) Corrosion engineering. McGraw Hill, New York, p 310
39. Jones DA (1996) Principles and prevention of corrosion. Prentice Hall, Upper Saddle River, p 120
40. Koehler JS (1949) Phys Rev 75:106
41. Landauer R (1951) Phys Rev 82:520
42. Landauer R (1954) Phys Rev 94:1386
43. Baxter WJ (1974) J Appl Phys 45:4692